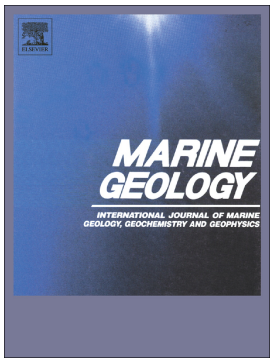

Giant depressions on the Chatham Rise offshore New Zealand – Morphology, structure and possible relation to fluid expulsion and bottom currents

Ingo Klaucke, Sudipta Sarkar, Jörg Bialas, Christian Berndt, Anke Dannowski, Ines Dumke, Jess Hillman, Stephanie Koch, Scott D. Nodder, Cord Papenberg, Jens Schneider von Deimling

PII: S0025-3227(17)30223-2
DOI: doi:10.1016/j.margeo.2018.02.011
Reference: MARGO 5765

To appear in: *Marine Geology*

Received date: 9 May 2017
Revised date: 23 January 2018
Accepted date: 26 February 2018

Please cite this article as: Ingo Klaucke, Sudipta Sarkar, Jörg Bialas, Christian Berndt, Anke Dannowski, Ines Dumke, Jess Hillman, Stephanie Koch, Scott D. Nodder, Cord Papenberg, Jens Schneider von Deimling , Giant depressions on the Chatham Rise offshore New Zealand – Morphology, structure and possible relation to fluid expulsion and bottom currents. The address for the corresponding author was captured as affiliation for all authors. Please check if appropriate. Margo(2017), doi:10.1016/j.margeo.2018.02.011

Giant depressions on the Chatham Rise offshore New Zealand – morphology, structure and possible relation to fluid expulsion and bottom currents

Ingo Klaucke[#], Sudipta Sarkar[*], Jörg Bialas[#], Christian Berndt[#], Anke Dannowski[#], Ines Dumke[#], Jess Hillman[#1], Stephanie Koch[#], Scott D. Nodder[§], Cord Papenberg[#], Jens Schneider von Deimling[#2]

[#]*GEOMAR Helmholtz-Centre for Ocean Research Kiel, Wischhofstrasse 1-3, 24148 Kiel, Germany*
[*]*Department of Earth and Climate Science, Indian Institute of Science Education and Research Pune, Maharashtra-411008, India*
[§]*NIWA, Private Bag 14-901, Kilbirnie, Wellington 6241, New Zealand*

Abstract

Several giant seafloor depressions were investigated on the Chatham Rise offshore New Zealand using mainly bathymetric and seismic data, supplemented by sediment cores and reported porewater geochemistry data. The depressions have diameters of up to 11 km and occur on the southern flank of the Chatham Rise in water depths between 600 and 900 m, i.e. roughly underneath the location of the strongest thermal gradients of the Subtropical Front (STF) and characterized by eastward flowing currents. With up to 150 m of relief the depressions cut into post-Miocene deposits. Some of the depressions are partially filled with drift deposits that have similar seismic characteristics as the surrounding sediments and consist of alternations of silty muds and silts. Seismic profiles also show completely filled depressions that no longer have a bathymetric expression. Despite several pipe structures indicating vertical fluid flow, neither active fluid seepage nor indications for past fluid seepage are present at the seafloor of the Chatham Rise. Also, both pore water geochemistry and geophysical data do not show indications for an existing or past gas hydrate system in the area. Instead, seismic data suggest widespread polygonal faulting and the presence of silica diagenetic fronts. The release of mineral-bound water during silica diagenesis or fluid expulsion during sediment compaction can explain the presence of vertical fluid flow features but not the giant depressions themselves. Instead, the depressions are interpreted as the result of scouring by strong bottom currents for which fluid venting may have created the nucleation points.

1 now at: GNS Science, Lower Hutt, New Zealand
2 now at: Institute of Geosciences, University of Kiel, Otto-Hahn-Platz 1, 24118 Kiel, Germany

Keywords: silica diagenesis, porewater expulsion, Chatham Rise, seafloor morphology, fluid flow system, current erosion

1. Introduction

Fluid venting on continental margins and the associated fluid flow systems attract much research (Berndt, 2005; Suess, 2014), because the emanating fluids are dominated by methane which is a potent greenhouse gas (Lashof and Ahuja, 1990). As a consequence, features of fluid venting and subsurface fluid flow are frequently discussed in terms of their possible impact on climate change (Judd et al., 2002; Svensen et al., 2004; Westbrook et al., 2009; Davy et al., 2010). The development of a fluid-flow system, however, requires a number of conditions in order to be established (Berndt, 2005; Talukder, 2012; Suess, 2014). Sufficient quantities of fluid need to be present and favourable pathways, such as permeable layers and faults need to exist. A driving mechanism (generally fluid overpressure generated by tectonic forces or sediment loading) is also required. Typical fluid sources consist of hydrocarbons originating from the thermal or biological degradation of organic matter within sediments (MacDonald, 1983), the diagenetic transformation of clay minerals in argillaceous sediments (Hensen et al., 2004), the expulsion of pore water during sediment compaction (Berndt et al., 2012), and the release of mineral-bound water during silica diagenetic transformation in siliceous sediments (Davies et al., 2008).

Determining the presence of a fluid flow system, and especially the type and origin of the fluid is difficult without direct observation and sampling of fluids emanating at the seafloor or within boreholes. Fluid venting, i.e. the escape of fluids at the seafloor, generally results in distinct seafloor morphologies (mounds or pockmarks) or specific seafloor properties such as increased backscatter intensity in sidescan sonar or multibeam backscatter data, all of which point to the existence of a fluid flow system (Suess, 2014 and references therein), even if fluid emissions are not observed. The same is true for specific features in seismic reflection profiles such as the presence of a bottom-simulating reflector (BSR), pipe structures, chimneys, wipe outs, or enhanced seismic reflections and bright spots (Berndt, 2005). Many fluid flow systems in deep-water sedimentary systems have been identified worldwide based on these characteristics.

Here, we report on a combined geophysical-geochemical study of the southern flank of the Chatham Rise (Fig. 1), east of New Zealand's South Island, an area where large seafloor depressions have been interpreted as giant pockmarks formed by the massive release of methane from gas hydrates (Davy et al., 2010). We wanted to test the hypothesis that massive methane release from these large depressions was primed by substantial amount of methane hydrate dissociation. We collected a comprehensive array of geophysical data over the large depressions in order to find evidence of gas hydrates and an associated fluid flow system (e.g. Berndt, 2005; Somoza et al., 2014). We visited all three areas highlighted by Davy et al. (2010) but focus here specifically on the easternmost site with the largest depressions, for which we show that despite some indications of focused fluid flow in the subsurface, our comprehensive dataset could not confirm the presence of a methane hydrate system in this area. Instead, our analysis of seafloor acoustic imaging and high-resolution seismic data supplemented by reported pore water geochemistry (Coffin et al., 2013) from this region suggests that the southern flank of the Chatham Rise is affected by fluid flow fuelled by silica diagenesis and porewater expulsion during sediment compaction, and that the large depressions are the result of repeated phases of current erosion and subsequent sediment infilling.

2. Geological setting

The Chatham Rise is part of the mainly submerged Zealandia continent (Mortimer et al., 2017) and constitutes a roughly 200 km wide ridge extending in a West-East orientation for more than 1000 km east of South Island, New Zealand (Fig. 1). It is bounded in the north by the much deeper Hikurangi Plateau and separated from the Campbell Plateau by the Bounty Trough in the south (Wood et al., 1989; Nodder et al., 2012). The Chatham Rise is relatively flat-topped with an average water depth around 400 metres, steep northern and slightly gentler southern flanks. Three main shallower shelf areas occur on the Chatham Rise; Mernoo and Veryan Banks in the West and the emergent Chatham Islands shelf in the East (Fig. 1).

Starting in the Permian the northern side of the Chatham Rise formed a convergent margin of Gondwana (Wood and Davy, 1994; Sutherland, 1999). Subduction stopped in the Late Cretaceous due to the collision of the Chatham Rise with the buoyant, young Hikurangi Plateau (Bradshaw, 1989; Davy and Wood, 1994; Davy et al., 2008). Although the Bounty Trough bounding the Chatham Rise to the South could also represent a back-arc basin, seismic velocities in the area indicate the presence of up to 9 km thick continental crust that

was probably thinned by the rifting and the separation of Zealandia and Antarctica (Carter and Carter, 1993; Grobys et al., 2007).

The Chatham Rise poses a natural barrier for the northward movement of the Subtropical Front (STF) during glacial cycles (Sikes et al., 2002; Hayward et al., 2008) as well as during the modern day (Uddstrom and Oien, 1999; Sutton, 2001). The STF (Fig. 1) separates the southward-flowing subtropical East Cape Current from the north- and eastward-flowing extension of the Southland Current carrying sub-Antarctic waters (Sutton, 2001, 2003; Chiswell, 2002). During glacial cycles, the STF remained located along the southern flank of the Chatham Rise (Hayward et al., 2008) but moved up and down the flank, while in other open ocean parts of the Southern Ocean the STF moved 3-5° latitude northwards (Hayward et al., 2008; Bostock et al., 2015). The region of the STF is marked by high primary productivity (Bradford-Grieve et al., 1997; Chiswell et al., 2013). Productivity, however, drops within short distances away from the STF, especially in sub-Antarctic waters to the south, where productivity is limited by iron availability (Boyd et al., 1999) and organic matter flux and accumulation rates are rather low (Nodder and Northcote, 2001; Nodder et al., 2003). The possible location of the STF on the Chatham Rise during glacial times is indicated by a remarkable up to 50 m-high step in the bathymetric profile located in 900 m water depth (Davy et al., 2010) while the strongest thermal gradients at the southern boundary of the present-day STF are located in roughly 500 m water depth (Uddstrom and Oien, 1999; Sutton, 2001).

Relatively little is known about the Cenozoic sedimentation history of the Chatham Rise, which is mainly composed of Paleogene to Miocene chalk deposits (Wood et al., 1989) that overlie Mesozoic basement rocks (schist, greywacke, meta-sedimentary rocks). Some studies also report localized biogenic opal and chert occurrences (von Rad and Kudrass, 1984; Dersch and Stein, 1991). The chalk is draped by thin Quaternary deposits (typically < 10 m thick) of glauconite-rich, muddy sands and sandy muds, localized phosphorite nodules and gravelly sand deposits of mostly biogenic origin (Cullen, 1987; Nodder et al., 2012; Leduc et al., 2015). From Mid-Miocene times the rise of the Southern Alps shed terrigenous sediments onto the western Chatham Rise (Wood et al., 1989). The Chatham Rise also hosts multiple sites of intra-plate Plio-Pleistocene basaltic volcanism, in particular near the Veryan Bank and surroundings (Herzer et al., 1989; Nodder et al., 2012).

Previously, a sparse grid of multibeam bathymetric survey lines across the Chatham Rise allowed the identification of several large seafloor depressions ranging in size from a few hundred metres to up to 10 km in diameter (Nodder et al., 2009; Davy et al., 2010). Based on their location with respect to the STF, the presence of a seismic reflector interpreted as a BSR and the likely extent of the methane hydrate stability zone at glacial times, the depressions have been interpreted as the result of gas hydrate decomposition leading to a massive release of methane into the water column (Davy et al., 2010).

Three areas, each representing a typical set of seafloor depressions, are distinguished on the Chatham Rise (Nodder et al., 2009; Davy et al., 2010; Collins et al., 20111; Nodder et al., 2012). Small depressions of 100-200 m in diameter and several metres of relief height occur in 500-700 m of water depth on the southwestern flank of the Chatham Rise (Fig. 1), and are probably also related to fluid/biogenic gas escape from the seafloor (Davy et al., 2010). Hillman et al. (2015), however, did not find conclusive evidence for an origin of these depressions by gas escape and suggest groundwater seepage and structural controls as alternative explanations. Large coalescing depressions of a few km in diameter and 50 – 150 m in relief height Nodder et al., 2009; Davy et al., 2010;Waghorn et al., 2018) are present in 800-1000 m of water depth east of Veryan Bank (Fig. 1). The depressions are interpreted as the result of fluid expulsion due to large-scale subsurface sediment remobilisation and polygonal faulting (Waghorn et al., 2018). However, evidence for methane hydrates was not found. Finally, very large, ellipsoidal depressions, up to 10 km in diameter (Nodder et al., 2009; Davy et al., 2010; Hillman et al., 2017), have been reported in 800-1100 m of water depth around 178°30'E on south Chatham Rise (Fig. 1)

3. Methods and data

A large geophysical, geological and geochemical dataset was acquired during RV SONNE cruise SO226 in austral summer 2013 (Bialas et al., 2013) at three working areas between 175° E and 179° E along the southern flank of the Chatham Rise (Fig. 1). Data acquired around 178°30' E used specifically for this study include multibeam bathymetry and backscatter data, 2D multi-channel seismic data, ocean bottom hydrophone data (OBH), piston and multi-corer sediment samples, as well as deep-towed sidescan sonar and echosounder data.

2D multi-channel seismic data were acquired using a short streamer with 137.5 m active length and 55 m lead-in. For most seismic reflection profiles a GI-gun source with 45/45 in^3 volume was used at 3 s shot interval resulting in seismic frequencies between 40 and 450 Hz and a signal penetration of 1.5-2 s two-way-travel-time (TWT). Some profiles were acquired using a 105/105 in^3 source with a 7 s shot interval generating frequencies from 25 Hz to 380 Hz but with no discernible improvement in signal penetration. Data processing included crooked line binning to 1.56 m bin size and zero-phase 6 Hz low-cut frequency filtering. A spatial median filter in the frequency domain attenuated anomalous amplitude noise and linear radon transformation reconstructed offsets for linear noise suppression. Normal move-out and stacking was applied before post-stack Kirchhoff time-migration using velocities below seafloor ranging from 1540 m s^{-1} at the seafloor to 3000 m s^{-1} at 3000 m subseafloor depth, based on a velocity model derived from OBH data. Interpretation of the seismic data was carried out using the IHS Kingdom Suite software. Chronostratigraphic correlations are based on sparse regional seismic profiles (Fig. 1) and correlation with drill holes and in particular the Resolution-1 industry well (Milne et al., 1975), DSDP hole 594 (Lewis et al., 1986) and IODP hole 1352 (Expedition 317 Scientists, 2011). The regional seismic lines (Wood et al., 1989) are of varying age, quality and sub-bottom penetration. Stratigraphic correlation consequently had to rely on seismic facies matching and TWT correlations.

Bathymetric data were acquired with a hull-mounted Simrad EM120 system (12 kHz) and a Seabeam 3050 system (50 kHz) that was mounted under the ship's moonpool. The Seabeam system allowed mapping of the water column and was tuned for the highest resolution to detect gas bubble flares across the entire swath. Bathymetric data processing using MB-system produced a grid with 25 m cell size (Fig. 2). Multibeam backscatter data of the Simrad EM120 system resulted in a compensated backscatter mosaic (Hillman et al., 2017) after processing the data with the SonarScope® Software developed at Ifremer, France. Additional instrumentation to search for active or recently active seepage included deep-towed sidescan sonar operating at 75 kHz and the primary 18 kHz signal of a parametric, hull-mounted echosounder system with the latter being operational throughout the survey.

Sediment sampling was carried out using a piston corer with 9 m-long barrels, a 3 m gravity corer and a deep-ocean multi-corer with 70 cm-long barrels (Coffin et al., 2013). Most multi-corer stations were co-located with piston core stations in order to sample the sediment-water interface. Core locations were positioned using an ultra-short baseline system providing an

accuracy of 1% of the water depth with the pinger transducer attached to the coring wire 50 m above the corer head. Geochemical analyses, including sulphate, chloride, dissolved inorganic carbon and methane, were carried out onboard (Coffin et al., 2013).

4. Results

4.1 Seismic units

Deposits within the study area show different units, based on lateral reflection continuity and amplitude (Fig. 3). We define six different seismic units (Unit I-VI). The lowermost Unit VI is poorly imaged with low amplitudes. Some reflections indicate faint onlap relationships onto an older unit. The top of Unit VI is marked by a strong, laterally continuous reflection of normal polarity that can be traced throughout the study area and marks an erosional unconformity. Unit VI has been interpreted as the sedimentary acoustic basement, i.e. the unit that is generally beyond the penetration of our data. Overlying Units V and IV show laterally continuous, parallel reflections that have only weak amplitudes in Unit V while amplitudes in Unit IV are strong. Within Unit IV lens-shaped packages with incoherent reflections are present, in particular towards the East of the study area. While the change from Unit V to Unit IV is gradational with poor lateral continuity, Unit IV is bound at the top by strong, continuous reflections that are traceable across the study area. Lateral tracing of these reflections towards the DSDP, IODP and industry drill holes (Figs. 1 and 4) suggests the top of Unit IV most likely corresponds to the top of the Palaeocene. The boundary between the Units III and II is less well-defined due to lateral pinch out and truncation of reflectors. While Unit III is weakly to moderately reflective, Unit II shows well stratified, parallel and continuous reflections. Correlation with regional seismic lines (Fig. 4) suggests that the boundary between Units III and II most likely corresponds to a Late Eocene time marker. The top of Unit II shows erosional truncations with subsequent infill of convex-curved reflections forming lens-shaped depositional bodies. This unconformity has been tentatively dated as the Late Miocene. The seismic facies of the infill (Unit I; Figs. 3 and 5) is, however, similar to the seismic facies of Unit II but shows higher amplitudes towards the shallower parts of the Chatham Rise (Fig. 5).

4.2 Seismic anomalies

Several anomalies are present in the seismic data. Within Unit III lenticular bodies marked by high amplitude reflections at the top and the base are present within a low reflectivity matrix (Fig. 3). In these lenses the upper bounding reflection appears to be inversed with respect to

the seafloor polarity while the lower bounding reflection has normal polarity. Similar high amplitude reflections are present within Unit IV, but the lenticular shape is less pronounced (Fig. 3). Also, the entire column comprising Units IV-I shows widespread near-vertical faults (Fig. 6). Most of them are restricted to Unit III while others originate from Unit III and extend into Unit I.

Several locations within the Units III and II show columnar disruptions of the lateral continuity of reflections (Figs. 3, 7 and 8). Some of these are restricted to the lower part of Unit III (Fig. 8) while others extent from Unit III to Unit II (Figs 3 and 8). None of these features reaches the seafloor.

A laterally continuous zone with bright reflections occurs within the lower part of unit II (Figs. 5 and 7). The top of this zone is marked by a positive polarity reflection, which has a highly irregular geometry forming a series of flat-topped plateaus (Fig. 7). Reflections above these zones of bright reflection are slightly bent forming a wavy pattern (Fig. 7).

4.3 Seafloor depressions

Multibeam bathymetry data show several large seafloor depressions in water depths between 600 m and 920 m. The diameters of the depressions range from 3 km to 11 km (Fig. 2). The largest depressions (A-C) are found in the East of the study area and show an either well-rounded or highly irregular elliptical outline in plan-view. The long axis in these cases is oriented NW-SE and the depressions are up to 150 m deep with respect to the surrounding seafloor. Other depressions (E-G) are crescent-shaped in plan-view with the apex consistently pointing south-westward. The rim of the depressions is either level with the surrounding seafloor or gradually steepening. Seismic profiles across the depressions show erosional truncations of reflections abutting against the depression and partial filling of some of the depressions with more recent deposits (Unit I, Figs. 3 and 5). For most of the depressions not only the western margin but also the northern and southern margins cut deeply into the pre-existing strata while the eastern margin is less steep. A few more infilled depressions exist outside of the present erosive seafloor depressions. They are filled with well-stratified deposits showing onlap relationships with the basal unconformity (Fig. 3), while the internal reflectors of the infill of the present seafloor depressions are convex-upward shaped (Fig. 5). The southwestern part of study area shows widespread erosion (Fig. 6) with evidence for present or past seafloor depressions.

4.4 Seafloor deposits and other observations

Sediment coring of Unit I (Fig. 2) revealed the presence of sandy mud to sand deposits over much of the study area. Core PC33 taken outside and to the southwest of depression A shows olive-grey sand and silt grading to grey silt and unconformably overlying lithified calcareous ooze that is interpreted as dating from the Miocene (Cullen, 1987). The calcareous ooze required unusually high pull (87 kN) to retrieve a 9-m long piston corer that apparently penetrated 4.5 metres. The presence of lithified calcareous ooze close to the seafloor is also expected for the base of large depression A, where Miocene strata of Unit II outcrop (Fig. 3) and where a 6-m long piston core could not be retrieved with 152 kN of pull. Two cores from the northern, shallower portion of the study area (PC45 and PC57) show the presence of up to 1-m thick olive grey sandy silt that grades downward into olive grey silt with traces of bioturbation and glauconite accumulations. For these cores Miocene chalk was not reached although core penetration was greater than for core PC33 taken further to the South and downslope on the Chatham Rise.

Neither the 18 kHz sediment echosounder nor the multibeam water column imaging showed gas flares in the water column. A deep-towed sidescan sonar survey across depressions A and B showed medium backscatter intensity throughout the survey area except for the rim of the depressions that are highlighted by some patches of higher backscatter intensity and rim-parallel bands of high and low backscatter that are also visible on multibeam backscatter data (Fig. 9).

5. Discussion

5.1. Fluid flow processes and sea floor morphology

Based on limited bathymetric data and a few isolated seismic and parametric echosounder (Parasound) profiles that did not cross the depressions, Davy et al. (2010) interpreted the large depressions on the southern flank of Chatham Rise as the result of massive gas hydrate dissociation during glacial cycles. Although the theoretical base of the hydrate stability zone coincides with the base of some of the large depressions, there are no indications for a gas hydrate BSR in the newly collected and more extensive seismic data (this study). The Parasound profile with high-amplitude reflections interpreted as a BSR by Davy et al., (2010) is located more than 300 km further west (west of Veryan Bank, Fig. 1) than the presently investigated large depressions. However, a SO226 seismic profile run over the same location

did not confirm the presence of a BSR in that area either (Bialas et al., 2013). Additional water column data did not reveal the presence of gas bubble streams during the SO226 survey, although this does not preclude their existence at other geological times. Cold seeps can be long-lived features that are active at least intermittently for thousands to hundreds of thousands of years (Teichert et al., 2003; Liebetrau et al., 2010; Levin et al., 2016), which generally results in the formation of massive authigenic carbonate precipitates. Sidescan sonar data from the Chatham Rise depressions, however, do not show elevated backscatter intensities that are indicative of authigenic carbonate precipitates and therefore fossil cold seeps (Sahling et al., 2008). On the other hand, gas hydrate dissociation would have to have been particularly vigorous to create the large depressions observed on Chatham Rise and consequently could likely have prevented the formation of authigenic carbonate crusts (Luff et al., 2004).

However, geochemical data derived from sediment cores indicated neither a vertical methane flux into the water column nor the presence of methane in the upper <10-m deep sediments (Coffin et al., 2013). Porewater geochemical profiles show little variation between sites within and the reference core outside of the depressions. Sulphate profiles show no to minimal decrease with depth, with sediment methane concentrations being only slightly above the limit of detection. The sulphate to methane transition zone consequently lies several tens of metres below seafloor, which precludes the presence of a reservoir of mobile methane within reach of our seismic data. Although few isolated bright spots are present in the seismic sections, most of them have positive polarity. Therefore, seismic indications for pervasive gas accumulations at depth are absent. If substantial amounts of methane hydrates dissociated during the last glacial cycles, as suggested by Davy et al. (2010), either gas hydrates or free gas should still be present in the subsurface. This is because the region is now at a greater water depth that favours hydrate formation, and varying sealevel or changes in bottom water temperatures will only shift the gas hydrate stability field up or down but would not lead to a complete disappearance of the hydrate system. If a well-sealed hydrate system exists presently at depth, it seems highly unlikely that it produced vigorous fluid expulsion at glacial times.

An essential component for the establishment of a gas hydrate system is the availability of free gas such as methane. The southern flank of the Chatham Rise shows high surface productivity that could have facilitated accumulation of organic matter and production of biogenic methane. Organic matter burial, however, appears to be patchy. Our data together

with previous studies (Nodder et al., 2003) indicate that organic matter preservation in the sediments is low, with contents of sedimentary organic carbon of 0.2-1.0% in surficial sediments (Nodder et al., 2003; Leduc et al., 2016). These factors are probably facilitated by low vertical organic matter flux, compared to the northern flank of the Chatham Rise due to enhanced recycling within the water column as inferred by Nodder and Northcote (2001). It is unlikely that conditions of primary productivity and organic matter preservation in the Pleistocene were different from today's scenario because the Chatham Rise acted as a barrier to the northward movement of the STF during glacial times (Sikes et al., 2002; Hayward et al., 2008). Without sufficient organic matter accumulation and preservation in the sediments biogenic methane generation is not possible. Conditions of organic matter preservation may, however, have been different in the distant geological past and thermal or biogenic gas could have derived from a deep source beyond the penetration depth of our seismic data. Our analysis of regional seismic lines used for stratigraphic correlations did not show indications of large gas accumulations at depth, although the study area is in the vicinity of a potential source rock (Wood et al., 1989). In their basin analysis Wood et al. (1989), however, concluded that the maturity of the source rock did not yet reach the oil window, which effectively precludes the formation of thermogenic gas. The conditions might be slightly altered further west, where Plio-Pleistocene volcanism has been reported (Herzer et al., 1989; Nodder et al., 2012). The lack of substantial methane in shallow sediments on the Chatham Rise likely limits gas hydrate formation, which consequently reduces the importance of gas hydrate in explaining the origin of the large depressions. Besides lacking evidence for present gas hydrate deposits, our seismic data analysis also proved that it is unlikely that a hydrate system existed on the Chatham Rise during glacial times.

5.2 Subsurface evidence for fluid flow

Despite the absence of strong evidence for subsurface gas the seismic data show pipe structures that are indicative of vertical fluid flow. The pipe structures appear to be preferentially rooted at the top of Units IV, with some also located higher up in the stratigraphic sequence (Figs. 3, 7 and 8). The fluids that caused these features most likely had a different origin than methane-rich fluids derived from organic matter degradation. Three diagenetic processes could have produced fluids that formed the observed fluid migration features.

The first possible source is mineral-bound water that is released during diagenetic transformations of clay minerals. The transformation of smectite to illite liberates minerally-bound water that has been proposed to play a role in the fluid flow system in the Gulf of Cadiz (Hensen et al., 2007) and offshore Costa Rica (Hensen et al., 2004), where it adds fluid to an existing gas hydrate system (Schmidt et al., 2005). However, the onset of smectite-illite transition occurs at temperatures of 58-92°C (Freed and Pecor, 1989). Heat flow data are not available from the Chatham Rise, but Davy et al. (2010) argue for slightly elevated geothermal gradients of up to 40°C km^{-1} due to the Neogene volcanism, which corresponds to a depth below sea floor of 1.5 km. As our study area is relatively far away from known areas of Plio-Pleistocene volcanism on the rise (Herzer et al., 1989; Collins et al., 2011), the geothermal gradient is probably less than 40°C km^{-1} and the corresponding onset of smectite-illite transition would occur even deeper. In fact, this transition would likely be too deep for the penetration of our seismic data. Furthermore, we do also do not observe pipe structures in the lower most Units V and VI that would point towards a deeper fluid source. Although smectite-illite transformation cannot be excluded as an origin of fluids, we consider it an unlikely source for the observed fluid expulsion features in the shallow subsurface of the Chatham Rise.

The second possible source is water that is expelled during the formation of polygonal fault systems. Although it is not entirely clear what the mechanisms of this process are, it has been demonstrated that formation of polygonal faults in fine-grained sediments is the result of sediment contraction (Cartwright and Lonergan, 1996) and is intrinsically linked to fluid expulsion (Berndt et al., 2012). Sub-vertical faults are widespread on the Chatham Rise (Fig. 6; Wood et al., 1989; Barnes, 1994) and are interpreted here as being part of a polygonal fault system, similar to those shown by Waghorn et al. (2018) in the same stratigraphic units further west of our study area. They are also widespread on the adjacent Canterbury shelf, as discussed by Hillman et al. (2015). Even though the origin of the observed faults cannot be constrained beyond doubt, it is most likely that the faults provided pathways for fluid expulsion through the Chatham Rise Paleogene sedimentary sequence.

The third potential source for fluids is the transformation of opal-A (amorphous) to opal-CT (cristobalite and tridymite) as well as the transformation of opal-CT to quartz which also liberates minerally-bound water (Hesse, 1989). Several studies have attributed BSRs to silica transformations in a number of different settings including the Bering Sea (Hein et al., 1978),

Sea of Japan (Kuramoto et al., 1992; Lee et al., 2003), Norwegian Sea (Berndt et al., 2004), Faroe-Shetland channel (Davies et al., 2008), and Scotia Sea, offshore Antarctica (Somoza et al., 2014). The latter case not only involved subsurface features but also seafloor features such as mounds or depressions, although these may also be explained by a co-existing gas-hydrate fluid flow system (Somoza et al., 2014).

On the southern flanks of the Chatham Rise an irregular diagenetic front in the form of plateau-like, high-amplitude zones (Figs. 5, 7 and 8) is present in the seismic data and is interpreted as representing the transformation of opal-A to opal-CT. We interpret the irregular, positive-polarity top of the high-amplitude zone as the result of varying advancement of the opal-A to opal-CT conversion. Where it moves upward relative to the surrounding regions, the overlying strata gently sink down, giving rise to small amplitude folds (Fig. 7). Similar seismic expression is known from the North Atlantic and can be explained by silica diagenetic transformation (Davies, 2005). The transformation of opal-A to opal-CT is a slow process and typically takes place at temperatures between 18-56°C (Botz and Bohrmann, 1991 and references therein) while the opal-CT to quartz conversion requires temperatures of 55-110°C (Murata et al., 1977). However, opal-CT precipitates at temperatures below 4°C if the host sediment is extremely poor in clay minerals (Botz and Bohrmann, 1991; Bohrmann et al., 1994). The Eocene (corresponding to Unit III) was a time of widespread silica deposition throughout the global ocean (McGowran, 1989) including eastern South Island, New Zealand, where a Late Eocene marine diatomite is locally exposed onshore (Edwards, 1991). The western part of the Chatham Rise experienced Neogene volcanism (Herzer et al., 1989) that probably resulted in elevated thermal gradients for the area. The opal-A/opal-CT transformation consequently would have started with less than 500 m of overburden. Basin-fill sedimentation rates in the Chatham Rise study area are reasonably well-constrained with calculated rates based on seismic profiles in the order of ~10 m Ma^{-1} for the Palaeocene-Oligocene, rising to ~20 m Ma^{-1} in the Miocene (Wood et al., 1989). Eocene-Miocene accumulation rates in the Southern Ocean are as low as 3 m Ma^{-1} (Brewster, 1980) while deep-water Quaternary sedimentation rates in the Chatham Rise region range between 10 m Ma^{-1} and 100 m Ma^{-1} with most values between 20 m Ma^{-1} and 30 m Ma^{-1} (Lean and McCave, 1998; Carter et al., 2000; Ronge et al., 2015). In our study area, the thickness of Eocene units averages 0.2 s TWT, which corresponds to 250-300 m. At the latest, after the time of the geographically widespread mid-Oligocene unconformity (Marshall

paraconformity, Fulthorpe et al., 1996), the silica deposits would have reached the depth of the opal-CT transformation zone and released fluid into the overlying sediments.

In the absence of other suitable explanations, silica transformation is suggested to have fuelled the fluid flow system that is apparent in the Palaeogene-Neogene sedimentary succession on the Chatham Rise. Whether this fluid flow system is still active today is unclear but the Eocene deposits are still located within the temperature range for opal A/opal-CT transformation. Coffin et al. (2013) showed one core (PC51) with significant freshening of pore water. This is in agreement with the idea that some of the observed fluid migration is fuelled by diagenetic transformation from opal-A to opal-CT, because this process releases fresh water (Hesse, 1989). In contrast, sediment contraction during polygonal faulting would release pore water with normal chlorinity.

Silica transformation has a profound effect on several submarine features including soft sediment deformation and differential compaction folds (Davies, 2005; Davies et al., 2006). The latter appears to be present on the Chatham Rise as well. At several locations lens-shaped bodies with curved upper and lower bounding reflections are present at the base of Unit III and possibly within Unit IV (Fig. 3). These lenses are interpreted to be the result of differential compaction due to either laterally varying degrees of opal-A in the original deposits or varying degrees and rates of silica diagenesis due to differences in sediment composition. The rates of silica diagenesis depend strongly on sediment composition (Kastner et al., 1977). Opal-A to opal-CT transformation also results in loss of porosity and increases in bulk density causing a positive acoustic impedance contrast. There is enhanced loss of porosity where the diagenetic front advances upward relative to the surrounding regions causing minor subsidence of the overlying strata (Davies, 2005).

A clear correlation between the lens-shaped bodies or the vertical fluid-flow pipes and the depressions could not be established. It is possible that many pipe structures were not imaged in the 2D-seismic data as the data coverage is low, but such pipe structures would have to be small compared to the seafloor depressions. The observed fluid pipes are not commensurate with the size of the giant depressions. Fluid pipes carrying mainly water released from silica diagenesis and/or polygonal faulting can, in the best case, create smaller pockmarks and irregularities at the seafloor that provide obstacles to bottom currents. Fluid flow alone was

consequently neither the only nor the dominant process that formed the seafloor depressions, which therefore require a different explanation.

5.3. Submarine erosion and seafloor morphology

Possible alternative origins for giant depressions include scouring by currents (Collins et al., 2011; MacDonald et al., 2011) or collapse of sediment layers following dissolution at depth (Somoza et al., 2003; Leon et al., 2010; Garcia et al., 2016). Currents on the Chatham Rise are steady and flow eastward with up to 0.2 m/s and even stronger tidal flow components (Chiswell, 2002; Hadfield et al., 2007). Nodder and Northcote (2001) showed that currents were persistently eastwards on the southern flank of the Chatham Rise for over a year of near-bottom current meter data at 1000 m water depth, 500 m above the seafloor, from 1996-97, with mean and maximum speeds of 0.11±0.01 and 0.26 m/s, respectively. These currents are vigorous enough to transport grains of up to 2 mm in diameter and are just strong enough to erode small non-cohesive grains of 0.05 – 0.2 mm in diameter, i.e very fine to fine sand. A marked step in the bathymetry corresponding to a separation between weakly and moderately backscattering surface deposits (Fig. 9) could represent the paleo-position of the STF (Davy et al., 2010). This zone is now located south of the large depressions and sandy deposits have been retrieved from that area (Fig. 2; cores PC59, PC60; Coffin et al., 2013). During glacial cycles the STF is inferred to have remained at the southern flank of the Chatham Rise (Sikes et al., 2002; Hayward et al., 2008) but most likely moved up and down the flank (Davy et al., 2010). In addition, during glacial times the eastward flowing current at the southern boundary of the STF was probably even stronger because temperature contrasts between the subantarctic and subtropical regions were greater. The strength of the subantarctic current system appears to be primarily controlled by the wind system (Böning et al., 2008), which would have been more intense with higher temperature contrasts. The eroding ability of the eastward-flowing current beneath the STF consequently is inferred to have been much higher during glacial times. Following on from this conclusion, we therefore also favour erosion by bottom currents as the process leading to the formation of the giant depressions.

The apex of the large seafloor depressions all point towards the West or West-southwest implying a general WSW-NNE current direction. This observation is in line with the asymmetrical profile of most of the depressions with a steep western and a gentler eastern flank - an observation also made by Collins et al. (2011) further west on the Chatham Rise.

We therefore interpret the depressions as giant scours or giga flute-marks, considering that normally flutes are observed on decimetre scales (Kuenen, 1957).

Giant scours are mainly known from channel-lobe transition zones in deep-sea submarine fan environments (Wynn et al., 2002; MacDonald et al., 2011), where they are related to the hydraulic jump of channelized sediment gravity flows (Garcia, 1993). Erosion, including scouring, is also known for contour currents and related to high flow velocities and gravelly deposits (Masson et al., 2004; Rebesco et al., 2014). Giant scours, similar to those on Chatham Rise but with elongation in flow direction, have only been described from the Faroe-Shetland Channel (Stoker et al., 2003; Masson et al., 2004), where they appear to be recurrent features related to strong bottom currents in very coarse-grained, gravelly deep-sea sediments. Collins et al. (2011) showed both highly irregular and crescent-shaped depressions on the western Chatham Rise that they attributed to current erosion. Crescent-shaped giant depressions (Duarte et al., 2010; Garcia et al., 2016) that are similar in dimension to those encountered on the Chatham Rise have also been described in the Gulf of Cadiz, from where other more elongate or irregular depressions have also been reported (Leon et al., 2010). The depressions in the Gulf of Cadiz are interpreted to be the result of fluid-flow induced collapse structures that were subsequently reworked by bottom currents (Leon et al., 2010; Garcia et al., 2016).

A similar scenario may apply to the Chatham Rise. However, our seismic data do not provide indications of collapse structures. We consequently propose an evolution scenario in which fluid venting at the seafloor generated pockmarks (Fig. 10B) that have subsequently been significantly widened and deepened by strong, predominantly eastward-flowing currents within the STF (Fig. 10C). Therefore, the spatial relationship between fluid flow pipe structures and the seafloor depressions has been overprinted by erosion. One could speculate that eddies within the STF (Chiswell, 2001, Williams, 2004) played a role in creating depressions that are elongate in the across-current direction rather than down-current as for the Faroe-Shetland Channel. However, it seems unlikely that eddies are stable on geological time-scales unless there is interaction between the seafloor topography and the location of the eddies, i.e. that their location is controlled by the depression. The observation that more than two thirds of the perimeter of the large depressions show a steep flank is suggestive of the influence of stationary eddies. The partial infill of most of the depressions with sediment drift bodies (Unit I) also indicates that the formation of the depressions predates the infill. Erosion

of the depressions most likely reflects a more vigorous (most likely glacial) current regime (Fig. 10C) than the current regime at the time of the infill (Fig. 10D). Whether this latter current regime prevails today or whether it also represents past conditions can only be determined from long-term current measurements within the depressions and detailed geochronological studies of the infill sediments and the timing of the formation of the depressions themselves.

Conclusions

The southern flank of the Chatham Rise is characterized by large seafloor depressions ranging in size from 2-10 km across. They are elliptical or crescent-shaped with the long axis oriented predominantly N-S to NW-SE. The depressions are eroded into the most recent strata and reach as deep as the Late Miocene but they are also partially filled by more recent sediment drift deposits.

Indications for a present or past gas hydrate system (as suggested by Davy et al., 2010) could not be found. Instead, subsurface data show irregular, positive-polarity reflections that are interpreted as representing a diagenetic front associated with the conversion of opal-A to opal-CT, and a closely-spaced set of sub-vertical faults that are most likely part of a regional polygonal fault system (e.g. Waghorn et al., 2018). Both the opal-A/opal-CT transformation and the development of polygonal faults provided fluids for a weak fluid flow system that generated pipe structures that are apparent in the seismic data. The fluid flow system, however, did not create the seafloor depressions as they are seen now but instead acted as weakened nucleation points for the initiation of erosion by bottom currents.

The morphology and internal structure of the large depressions suggest that they most likely originate from erosion by the eastward-flowing extension of the Southland Current and that they may represent giant scours or flute marks. Current erosion was possibly initiated by seafloor irregularities such as pockmarks created by fluid venting and may have been reinforced by eddies associated with the Subtropical Front, especially since the southern boundary of the frontal zone is characterised by strong thermal gradients and persistent eastward near-bottom currents. Current erosion and possibly sediment drift deposition within the depressions reflects past current flow conditions, with erosion most likely during glacial times.

The example of the Chatham Rise presented in this study shows that indications for fluid flow should be treated with care, as they may not always be related to methane gas nor have implications for the release of hydrate-bound methane impacting climate change.

Acknowledgements

We would like to thank masters, officers and crew for their excellent work during RV SONNE cruise SO226 for which the German Ministry of Education and Research (contract no. 03G0226), GNS Science, NIWA Core funding (Coasts & Oceans, Marine Physical Processes & Resources) and NSF provided funding. Rick Coffin (US Naval Research Laboratory, Texas A&M University Corpus Christi, USA) and his team are thanked for sediment piston core sampling during the cruise and for sharing their results and insights. Bryan Davy (GNS Science) is thanked for stimulating discussions, as is John Mitchell (NIWA) for coring assistance at sea, while thoughtful criticism by Marc de Batist, Luis Somoza and an anonymous reviewer helped improve the manuscript.

References

Barnes, P.M., 1994. Inherited structural control from repeated Cretaceous to Recent extension in the North Mernoo Fault Zone, western Chatham Rise, New Zealand." Tectonophysics 237, 27-46.

Berndt, C., 2005. Focused fluid flow in passive continental margins. Philos. Trans. R. Soc. London A 363, 2855-2871.

Berndt, C., Bünz, S., Clayton, T., Mienert, J., Saunders, M., 2004. Seismic character of bottom simulating reflectors: examples from the mid-Norwegian margin. Mar. Petrol. Geol. 21, 723-733.

Berndt, C., Jacobs, C., Evans, A., Gay, A., Elliott, G., Long, D., Hitchen, K., 2012. Kilometre-scale polygonal seabed depressions in the Hatton Basin, NE Atlantic Ocean: Constraints on the origin of polygonal faulting. Mar. Geol. 332, 126-133.

Bialas, J., Klaucke, I., Mögeltönder, J. (eds.), 2013. RV SONNE Fahrtbericht / Cruise Report SO226 - CHRIMP CHatham RIse Methane Pockmarks, 07.01. - 06.02.2013 / Auckland – Lyttelton, 07.02. – 01.03.2013 / Lyttelton - Wellington . GEOMAR Report, N. Ser. 007 . GEOMAR Helmholtz-Zentrum für Ozeanforschung, Kiel, 126 p. DOI 10.3289/GEOMAR_REP_NS_7_2013.

Böning, C.W., Dispert, A., Visbeck, M., Rintoul, S.R., Schwarzkopf, F.U., 2008. The response of the Antarctic Circumpolar Current to recent climate change. Nature Geosci. 1, 864-869.

Bohrmann, G., Abelmann, A., Gersonde, R., Hubberten, H., Kuhn, G., 1994. Pure siliceous ooze, a diagenetic environment for early chert formation. Geology 22, 207-210.

Bostock, H.C., Hayward, B.W., Neil, H.L., Sabaa, A.T., Scott, G.H., 2015. Changes in the position of the Subtropical Front south of New Zealand since the last glacial period. Paleoceanography 30(7), 824-844.

Botz, R., Bohrmann, G., 1991. Low-temperature opal-CT precipitation in Antarctic deep-sea sediments: evidence from oxygen isotopes. Earth Planet. Sci. Lett. 107, 612-617.

Boyd, P., LaRoche, J., Gall, M., Frew, R., McKay, R.M.L., 1999. Role of iron, light, and silicate in controlling algal biomass in subantarctic waters SE of New Zealand. Jour. Geophys. Res. Oceans 104, 13395-13408.

Bradford-Grieve, J.M., Chang, F.H., Gall, M., Pickmere, S.F.R., 1997. Size-fractionated phytoplankton standing stocks and primary production during austral winter and spring 1993 in the Subtropical Convergence region near New Zealand. NZ Jour. Mar. Fresh. Res. 31, 201-224.

Bradshaw, J.D., 1989. Cretaceous dispersion of Gondwana: Continental and oceanic spreading in the southwest Pacific-Antarctic sector, In: Thomson, M.R.A. et al. (eds.) Geological Evolution of Antarctica, Cambridge Univ. Press, New York, 581-585.

Brewster, N.A., 1980. Cenozoic biogenic silica sedimentation in the Antarctic Ocean. Geol. Soc. Am. Bull. 91, 337-347.

Carter, L.T., Carter, R.M., 1993. Sedimentary evolution of the Bounty Trough: a Cretaceous rift basin, southwestern Pacific Ocean. South Pacific Sedimentary Basins. Sedimentary Basins of the World 2, 51-67.

Carter, L., Neil, H.L., McCave, I.N., 2000. Glacial to interglacial changes in non-carbonate and carbonate accumulation in the SW Pacific Ocean, New Zealand. Palaeogeo. Palaeoclim. Palaeoeco. 162, 333-356.

Cartwright, J.A., Lonergan, L., 1996. Volumetric contraction during the compaction of mudrocks: a mechanism for the development of regional-scale polygonal fault systems. Basin Res. 8, 183-193.

Chiswell, S.M. , 2001. Eddy energetics in the subtropical front over the Chatham Rise, New Zealand. NZ Jour. Mar. Freshwater Res. 35, 1-15.

Chiswell, S.M., 2002. Temperature and salinity mean and variability within the Subtropical Front over the Chatham Rise, New Zealand. NZ. J. Mar. Freshw. Res. 36, 281-298.

Chiswell, S.M., Bradford-Grieve, J., Hadfield, M.G., Kennan, S.C., 2013. Climatology of surface chlorophylla, autumn-winter and spring blooms in the southwest Pacific Ocean. Jour. Geophys. Res. Oceans 118, 1003-1018.

Chiswell, S.M., Bostock, H.C., Sutton, P.J., Williams, M.J., 2015. Physical oceanography of the deep seas around New Zealand: a review. NZ Jour. Mar. Freshw. Res. 49, 286-317.

Coffin, R.B., Boyd, T.J., Rose, P.S., Yoza, B., Milholland, L.C., Downer, R., Woods, S., 2013. Geochemical cruise report SO226/2 RV Sonne Chatham Rise Expedition. NRL/MR/6110—13-9472 https://www.netl.doe.gov/File%20Library/Research/Oil-Gas/methane%20hydrates/nt42878-geochemical-cruise-report.pdf (accessed 25.04.16).

Collins, J.A., Molnar, P., Sheehan, A.F., 2011. Multibeam bathymetry surveys of submarine volcanoes and mega-pockmarks on the Chatham Rise, New Zealand. NZ Jour. Geol. Geophys. 54, 329-339.

Cullen, D.J., 1987. The submarine phosphate resource on central Chatham Rise. Div. Mar. Freshwater Sci. Rep. 2, 22 p.

Davies, R.J., 2005. Differential compaction and subsidence in sedimentary basins due to silica diagenesis: A case study. Geol. Soc. Am. Bull. 117, 1146-1155.

Davies, R.J., Huuse, M., Hirst, P., Cartwright, J., Yang, Y., 2006. Giant clastic intrusions primed by silica diagenesis. Geology 34, 917-920.

Davies, R.J., Goulty, N.R., Meadows, D., 2008. Fluid flow due to the advance of basin-scale silica reaction zones. Geol. Soc. Am. Bull. 120, 195-206.

Davy, B., Hoernle, K., Werner, R., 2008. Hikurangi Plateau: Crustal structure, rifted formation, and Gondwana subduction history, Geochem. Geophys. Geosyst. 9, Q07004.

Davy, B., Pecher, I., Wood, R.A., Carter, L., Gohl, K., 2010. Gas escape features off New Zealand: Evidence of massive release of methane from hydrates. Geophys. Res. Lett. 37. L21309.

Davy, B., Wood, R.A., 1994. Gravity and magnetic modelling of the Hikurangi Plateau. Mar. Geol. 118, 139–151.

Dersch, M. and Stein, R., 1991. Paläoklima und paläoozeanische Verhältnisse im SW-Pazifik während der letzten 6 Millionen Jahre (DSDP-Site 594, Chatham Rücken, östlich Neuseeland). Geol. Rundschau 80, 535-556.

Duarte, J.C., Terrinha, P., Rosas, F.M., Valadares, V., Pinheiro, L.M., Matias, L., Magelhaes, V., Roque, C., 2010. Crescent-shaped morphotectonic features in the gulf of Cadiz (offshore SW Iberia). Mar. Geol. 271, 236-249.

Edwards, A.R. ed., 1991. The Oamaru Diatomite. Paleont. Bull. NZ Geol. Surv. 64, 171-244.

Expedition 317 Scientists, 2011. Site U1352. In Fulthorpe, C.S., Hoyanagi, K., Blum, P., Expedition 317 Scientists, Proc. IODP, 317: Tokyo (Integrated Ocean Drilling Program Management International, Inc.), doi:10.2204/iodp.proc.317.104.2011.

Freed, R.L., Peacor, D.R., 1989. Variability in temperature of the smectite/illite reaction in Gulf Coast sediments. Clay Miner. 24, 171–180.

Fulthorpe, C.S., Carter, R.M., Miller, K.G., Wilson, J., 1996. Marshall Paraconformity: a mid-Oligocene record of inception of the Antarctic circumpolar current and coeval glacio-eustatic lowstand? Mar. Petrol. Geol. 13, 61-77.

García, M.H., 1993. Hydraulic jumps in sediment-driven bottom currents. Jour. Hydraulic Eng. 119, 1094-1117.

García, M., Hernández-Molina, F.J., Alonso, B., Vásquez, J.T., Ercilla, G., Llave, E., Casas, D., 2016. Erosive sub-circular depressions on the Guadalquivir Bank (Gulf of Cadiz): Interaction between bottom current, mass-wasting and tectonic processes. Mar. Geol. 378, 5-19.

Grobys, J.W.G., Gohl, K., Davy, B., Uenzelmann-Neben, G., Deen, T., Barker, D., 2007. Is the Bounty Trough off eastern New Zealand an aborted rift? J. Geophys. Res. 112, B03103.

Hadfield, M.G., Rickard, G.J., Uddstrom, M.J., 2007. A hydrodynamic model of Chatham Rise, New Zealand. N.Z. Jour. Mar. Freshw. Res. 41, 239-264.

Hayward, B.W., Scott, G.H., Crundwell, M.P., Kennett, J.P., Carter, L., Neil, H.L., Sabaa, A.T., Wilson, K., Rodger, J.S., Schaefer, G., Grenfell, H.R., Li. Q., 2008. The effect of submerged plateaux on Pleistocene gyral circulation and sea-surface temperatures in the Southwest Pacific. Global Planet. Change 63, 309-316.

Hein, J.R., Scholl, D.W., Barron, J.A., Jones, M.G., Miller, J., 1978. Diagenesis of Late Cenozoic diatomaceous deposits and formation of the bottom simulating reflector in the southern Bering Sea. Sedimentology 25, 155-181.

Hensen, C., Wallmann, K., Schmidt, M., Ranero, C.R., Suess, E., 2004. Fluid expulsion related to mud extrusion off Costa Rica - a window to the subducting slab, Geology 32, 201-204.

Hensen, C., Nuzzo, M., Hornibrook, E., Pinheiro, L.M., Bock, B., Magalhães, V.H., Brückmann, W., 2007. Sources of mud volcano fluids in the Gulf of Cadiz—indications for hydrothermal imprint. Geochim. Cosmochim. Acta 71, 1232-1248.

Herzer, R.H., Challis, G.A., Christie, R H.K., Scott, G.H., Waters, W.A., 1989. The Urry Knolls, late Neogene alkaline basalt extrusives, southwestern Chatham Rise. Jour. R. Soc. NZ 19, 181-193.

Hesse, R., 1989. Silica diagenesis: origin of inorganic and replacement cherts. Earth-Sci. Rev. 26, 253-284.

Hillman, J.I.T., Gorman, A.R., Pecher, I.A., 2015. Geostatistical analysis of seafloor depressions on the southeast margin of New Zealand's South Island - Investigating the impact of dynamic near seafloor processes on geomorphology. Mar. Geol. 360, 70-83.

Hillman, J.I.T., Lamarche, G., Pallentin, A., Pecher, I.A., Gorman, A.R., Schneider, J., 2017. Validation of automated supervised segmentation of multibeam backscatter data from the Chatham Rise. Mar. Geophys. Res., doi:10.1007/s11001-016-9297-9.

Judd, A.G., Hovland, M., Dimitrov, L.I., Garcia Gil, S., Jukes, V., 2002. The geological methane budget at continental margins and its influence on climate change. Geofluids 2: 109-126.

Kastner, M., Keene, J.B., Gieskes, J.M., 1977. Diagenesis of siliceous oozes. I. Chemical controls on the rate of opal-A to opal-CT transformation—an experimental study. Geochim. Cosmochim. Acta 41, 1041–1059.

Kuenen, P.H., 1957. Sole markings of graded graywacke beds. Jour. Geol. 65, 231-258.

Kuramoto, S., Tamaki, K., Langseth, M.G., Nobes, D.C., Tokuyama, H., Pisciotto, K.A., Taira, A., 1992. Can Opal A/Opal-C/T BSR be an indicator of the thermal structure of the Yamato Basin, Japan Sea? Proc. Ocean Drill. Prog. Sci. Res. 127– 128, 1145–1151.

Lashof, D.A., Ahuja, D. R., 1990. Relative contributions of greenhouse gas emissions to global warming. Nature 344: 529-531.

Lean, C.M.B., McCave, I.N., 1998. Glacial to interglacial mineral magnetic and palaeoceanographic changes at Chatham Rise, SW Pacific Ocean. Earth Planet. Sci. Lett. 163, 247-260.

Leduc, D., Pilditch, C.A., Nodder, S.D., 2016. Partitioning the contributions of mega-, macro- and meiofauna to benthic metabolism on the upper continental slope of New Zealand: Potential links with environmental factors and trawling intensity. Deep Sea Research Part I: Oceanogr. Res. Papers 108, 1-12.

Leduc, D. Rowden, A.A., Torres, L.G., Nodder, S.D., Pallentin, A., 2015. Distribution of macro-infaunal communities in phosphorite nodule deposits on Chatham Rise, Southwest Pacific: Implications for management of seabed mining. Deep Sea Res. Part I: Ocean. Res. Papers 99, 105-118.

Lee, G.H., Kim, H.-J., Jou, H.-T., Cho, H.-M., 2003. Opal-A/Opal-CT phase boundary inferred from bottom-simulating reflectors in the southern South Korea Plateau, East Sea (Sea of Japan). Geophys. Res. Lett. 30, 2238.

Leon, R., Somoza, L., Medialdea, T., Hernandez-Molina, F.J., Vazquez, J.T., Diaz-de-Rio, V., Gonzalez, F.J., 2010. Pockmarks, collapses and blind valleys in the Gulf of Cadiz. Geo-Mar. Lett. 30, 231-247.

Levin, L.A., Baco, A.R., Bowden, D.A., Colaco, A., Cordes, E.E., Cunha, M.R., Demopoulos, A.W.J., Gobin, J., Grupe, B.M., Le, J., Metaxas, A., Netburn, A.N., Rouse, G.W., Thurber, A.R., Tunnicliffe, V., Van Dover, C.L., Vanreusel, A., Watling, L. 2016. Hydrothermal vents and methane seeps: rethinking the sphere of influence. Front. Mar. Sci. 3, 72 http://dx.doi.org/10.3389/fmars.2016.00072

Lewis, K.B., Bennett, D.J., Herzer, R.H., von der Borch, C.C., 1986. Seismic stratigraphy and structure adjacent to an evolving plate boundary, western Chatham Rise, New Zealand, Proc. Deep Sea Drilling Program, doi:10.2973/dsdp.proc.90.138.1986.

Liebetrau, V., Eisenhauer, A., Linke, P., 2010. Cold seep carbonates and associated cold-water corals at the Hikurangi Margin, New Zealand: New insights into fluid pathways, growth structures and geochronology. Mar Geol 272, 307-318.

Luff, R., Wallmann, K., Aloisi, G., 2004. Numerical modeling of carbonate crust formation at cold vent sites: significance for fluid and methane budgets and chemosynthetic biological communities. Earth Planet. Sci. Lett. 221, 337-353.

MacDonald, G.J., 1983. The many origins of natural gas, J. Petrol. Geol. 5, 341-362.

Macdonald, H.A., Wynn, R.B., Huvenne, V.A., Peakall, J., Masson, D.G., Weaver, P.P.E., McPhail, S.D., 2011. New insights into the morphology, fill, and remarkable longevity (> 0.2 my) of modern deep-water erosional scours along the northeast Atlantic margin. Geosphere 7: 845-867.

Masson, D.G., Wynn, R.B., Bett, B.J., 2004. Sedimentary environment of the Faeroe-Shetland Channel and Faeroe Bank channels, NE Atlantic, and the use of bedforms as indicators of bottom current velocity in the deep ocean. Sedimentology 51, 1–35.

McGowran, B., 1989. Silica burp in the Eocene ocean. Geology 17, 857-860.

Milne, A.D., Simpson, C., Threadgold, P., 1975. Well completion report Resolution, for BP, Shell, Todd Canterbury Service Limited. New Zealand open-file petroleum report 648. Crown Minerals, New Zealand.

Mortimer, N., Campbell, H.J., Stagpoole, M., Wood, R.A., Rattenbury, M.S., Sutherland, R., Seton, M., 2017. Zealandia: Earth's Hidden Continent. GSA Today 27, doi: 10.1130/GSATG321A.1

Murata, K.J., Friedman, I., Gleason, J.D., 1977. Oxygen isotope relations between diagenetic silica minerals in Monterey Shale, Temblor Range, California. Am. J. Sci. 277, 259–272.

Nodder, S., Bowden, D., Hewitt, J., 2009. New Zealand's Ocean Survey 20/20 programme: Understanding the relationships between seabed habitats and biodiversity using broadscale mapping, GeoHab 2009 conference abstracts, Geol. Surv. Norway, Trondheim, Norway.

Nodder, S.D., Bowden, D.A., Pallentin, A., Mackay, K., 2012. Seafloor habitats and benthos of a continental ridge: Chatham Rise, New Zealand (Chapter 56). In: P.T. Harris, E.K. Baker, eds., Seafloor Geomorphology as Benthic Habitat: GeoHab Atlas of seafloor geomorphic features and benthic habitats, Elsevier Insights, 763-776.

Nodder, S.D., Northcote, L.C., 2001. Episodic particulate fluxes at southern temperate mid-latitudes (42-45°S) in the Subtropical Front region, east of New Zealand. Deep Sea Res. Part I: Ocean. Res. Papers 48, 833-864.

Nodder, S.D., Pilditch, C.A., Probert, P.K., Hall, J.A., 2003. Variability in benthic biomass and activity beneath the Subtropical Front, Chatham Rise, SW Pacific Ocean. Deep Sea Res. Part I: Ocean. Res. Papers 50, 959-985.

Rebesco, M., Hernández-Molina, F.J., Van Rooij, D., Wåhlin, A., 2014. Contourite and associated sediments controlled by deep-water circulation processes: state-of-the-art and future considerations. Mar. Geol. 352, 111-154.

Ronge, T.A., Steph, S., Tiedemann, R., Prange, M., Merkel, U., Nürnberg, D., Kuhn, G., 2015. Pushing the boundaries: Glacial/interglacial variability of intermediate and deep waters in the southwest Pacific over the last 350,000 years. Paleoceanography 30, 23-38.

Sahling, H., Bohrmann, G., Spiess, V., Bialas, J., Breitzke, M., Ivanov, M.K., Kasten, S., Krastel, S., Schneider, R. 2008. Pockmarks in the Northern Congo Fan area, SW Africa: Complex seafloor features shaped by fluid flow. Mar. Geol. 249, 206-225.

Schmidt, M., Hensen, C., Mörz, T., Müller, C., Grevemeyer, I., Wallmann, K., Mau, S., Kaul, N., 2005. Methane hydrate accumulation in "Mound 11" mud volcano, Costa Rica forearc. Mar. Geol. 216, 83-100.

Sikes, E.L., Howard, W.R., Neil, H.L., Volkman, J.K., 2002. Glacial‐interglacial sea surface temperature changes across the subtropical front east of New Zealand based on alkenone unsaturation ratios and foraminiferal assemblages. Paleoceanography, 17(2), 1-13.

Somoza, L., León, R., Medialdea, T., Pérez, L.F., González, F.J., Maldonado, A., 2014. Seafloor mounds, craters and depressions linked to seismic chimneys breaching fossilized diagenetic bottom simulating reflectors in the central and southern Scotia Sea, Antarctica. Global Planet. Change 123, 359-373.

Stoker, M.S., Long, D., Bulat, J., 2003. A record of mid-Cenozoic strong deep-water erosion in the Faroe–Shetland Channel. In: Mienert, J., Weaver, P., (Eds.), European Margin Sediment Dynamics: Side-scan Sonar and Seismic Images. Springer, Berlin, pp. 145–148.

Suess, E., 2014. Marine cold seeps and their manifestation: geological control, biogeochemical criteria and environmental conditions. Int. Jour. Earth Sci. 103, 1765-1787.

Sutherland, R., 1999. Basement geology and tectonic development of the greater New Zealand region: an interpretation from regional magnetic data. Tectonophysics 308, 341-362.

Sutton, P.J.H., 2001. Detailed structure of the Subtropical Front over Chatham Rise, east of New Zealand, Jour. Geophys. Res. 106(C12), 31045-31056.

Sutton, P.J.H. 2003. The Southland Current: a subantarctic current. NZ Jour. Mar. Freshw. Res. 37, 645-652.

Svensen, H., Planke, S., Malthe-Sørenssen, A., Jamtveit, B., Myklebust, R., Eidem, T.R., Rey, S.S., 2004. Release of methane from a volcanic basin as a mechanism for initial Eocene global warming. Nature 429, 542-545.

Talukder, A.R., 2012. Review of submarine cold seep plumbing systems: leakage to seepage and venting. Terra Nova 24, 255-272.

Teichert, B.M.A., Eisenhauer, A., Bohrmann, G., Haase-Schramm, A., Bock, B., Linke, P., 2003. U/Th systematics and ages of authigenic carbonates from Hydrate Ridge, Cascadia Margin: Recorders of fluid flow variations. Geochim. Cosmochim. Acta 67, 3845-3857.

Uddstrom, M.J., Oien, N.A., 1999. On the use of high resolution satellite data to describe the spatial and temporal variability of sea surface temperatures in the New Zealand region. Jour. Geophys. Res. 104 (C9), 20729–20751.

Von Rad, U., Kudrass, H.-R., eds. 1984. Geology of the Chatham Rise phosphorite deposits east of New Zealand: Results of a prospection cruise with RV Sonne (1981). Geol. Jahrbuch D65, 252p.

Waghorn, K.A., Pecher, I., Strachan, L.J., Crutchley, G., Bialas, J., Coffin, R.B., Davy, B., Koch, S., Kröger, K.F., Papenberg, C., Sarkar, S., SO226 Scientific Party, 2018. Paleo-fluid

expulsion and contouritic drift formation on the Chatham Rise, New Zealand. Basin Res. 30, 5-19. DOI: 10.1111/bre.12237.

Westbrook, G.K., Thatcher, K.E., Rohling, E.J., Piotrowski, A.M., Palike, H. et al. (2009), Escape of methane gas from the seabed along the West Spitsbergen continental margin, Geophys. Res. Lett. 36, L15608.

Williams, M.J.M. (2004) Analysis of quasi-synoptic eddy observations in the New Zealand subantarctic, NZ Jour. Mar. Freshw. Res. 38, 183-194.

Wood, R.A., Andrews, P.B., Herzer, R.H., 1989. Cretaceous and Cenozoic geology of the Chatham Rise region, South Island, New Zealand. N.Z. Geol. Surv. Basin Stud. 3, 75 p.

Wood, R.A., Davy, B. 1994. The Hikurangi Plateau. Mar. Geol. 118, 153-173.

Wynn, R.B., Kenyon, N.H., Masson, D.G., Stow, D.A.V., Weaver, P.P.E., 2002. Characterization and recognition of deep-water channel-lobe transition zones. AAPG Bull. 86, 1441-1462.

Figure captions

Figure 1: Shaded-relief map (TOPEX data) of the Chatham Rise and adjacent area showing physiographic features and names used in the text. The shaded area depicts the position of the Subtropical Front according to Chiswell et al. (2015). Black arrows depict the flow direction of the Southland Current and its eastward extension, and red arrows the flow of the East Cape Current and the Wairarapa Eddy. Blue lines show regional seismic profiles (Wood et al., 1989) and intersecting line of RV SONNE SO226 cruise.

Figure 2: Shaded relief map of the southern flank of Chatham Rise showing several large seafloor depressions (labelled A-H). Location of 2D seismic profiles and sediment cores (PC = piston core, green stars = geochemistry cores) acquired during RV SONNE cruise SO226 are shown.

Figure 3: Multichannel seismic reflection profile crossing depression C and showing several vertical pipe structures and other dewatering features. The lens-shaped features of Unit III are interpreted as possible zones of incomplete opal-A to opal-CT transformation (see main text for discussion).

Figure 4: Chronostratigraphic correlation between NZ-80 seismic line and SO226-2000 line. TC = Top Cretaceous, TP = Top Palaeocene, TE = Top Eocene ad MP = Marshall Paraconformity (Fulthorpe et al., 1996) are based on correlation with Resolution-1 well and IODP hole 1352. TLM = Top of Lower Miocene and TM = Top Miocene are based on correlation with Resolution-1 and DSDP hole 594 (for profile and drill hole locations see figure 1). Yellow dotted lines and seismic units are adapted from Wood et al. (1989) and MOBIL 72-33 seismic line.

Figure 5: A. Multichannel seismic reflection profile across depression A on the southern Chatham Rise showing different depositional units. Profile location is shown in figure 2. B. Interpretative line-drawing highlighting different depositional unit (expected lithologies taken from Wood et al., (1989)). Interpretation of siliceous shale (porcellanite) of Unit II is based on our seismic interpretation and reports of chert occurrences by Wood et al., (1989) from dredge samples further upslope on the Chatham Rise, where Eocene beds are exposed or thinly

covered by recent sediments. A middle Oligocene Unconformity (Marshall Paraconformity) is not clearly seen in this section, therefore, the Oligocene-Miocene boundary is not shown.

Figure 6: Multichannel seismic profile showing many sub-vertical faults with only little displacement that are interpreted as polygonal faulting.

Figure 7: Seismic reflection profile showing a diagenetic front (yellow dotted line) separating zones with high amplitude reflections from low amplitude reflections above. The red arrows mark the relative upward advancement of the diagenetic transformation boundary (opal-A to opal-CT) from the adjacent diagenetic front showing positive polarity. Line location is provided in Figure 5a.

Figure 8: Multichannel seismic reflection profile across the eastern edge of depression A showing a strong reflection with positive polarity and poor lateral continuity that has been interpreted as a diagenetic signal of opal-A to opal-CT transformation front. Profile location is shown in figure 2.

Figure 9: Combined bathymetry and backscatter mosaic of the eastern Chatham Rise area. High backscatter is light-coloured. White arrows highlighting a marked step in bathymetry depict the boundary between strong seafloor erosion in the southwest and recent sandy-silty deposition in the northeast.

Figure 10: Conceptual sketch showing the presumed evolution of the seafloor depressions on the Chatham Rise. A. Deposition and subsequent burial of biogenic silica deposits (grey shaded area) with possibly some fluid release due to sediment compaction and polygonal faulting. B. Diagenesis of biogenic silica. The biogenic opal-A rich layers reprecipitate as opal-CT. The diagenetic transformation boundary (OCT) moves up the stratigraphic section in an irregular fashion, forming plateaus where the OCT advances ahead of the surrounding areas. Strata overlying the plateaus sink down since opal-CT is denser than opal-A. 'L' represents lensoid units where opal-A remained unconverted. Fluid pipes emanate from the top of the diagenetic transformation boundary (OCT). C. Scouring by strong bottom currents (probably during glacial times). D. Infilling of the depressions by drift deposits due to waning bottom currents, especially during interglacial times.

Highlights

- Large seafloor depressions with diameters of up 10 km across have been mapped on the southern Chatham Rise, New Zealand.
- Seismic reflection data show scarce indications for vertical fluid flow but no clear link between fluid flow and depressions.
- Methane gas or methane hydrates appear to be absent on the southern Chatham Rise.
- Seismic evidence suggests that vertical fluid flow was likely fuelled by polygonal faulting and silica diagenesis
- The depressions are the results of erosion and sediment drift deposition of bottom currents associated with the Subtropical Front.

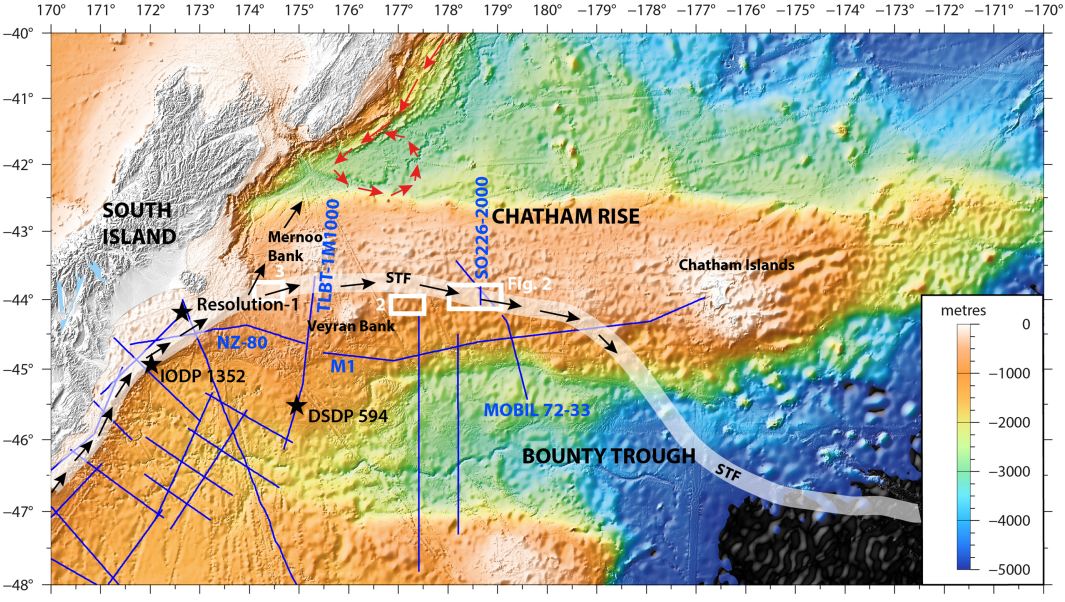
170°
171°
172°
173°
174°
175°
176°
177°
178°
179°
180°
−179°
−178°
−177°
−176°
−175°
−174°
−173°
−172°
−171°
−170°
−40°
−41°
−42°
−43°
−44°
−45°
−46°
−47°
−48°
SOUTH ISLAND
Mernoo Bank
TLBT-1M1000
SO226-2000
CHATHAM RISE
Chatham Islands
STF
Fig. 2
Resolution-1
Veyran Bank
NZ-80
M1
IODP 1352
DSDP 594
MOBIL 72-33
BOUNTY TROUGH
STF
metres
0
−1000
−2000
−3000
−4000
−5000

Figure 1

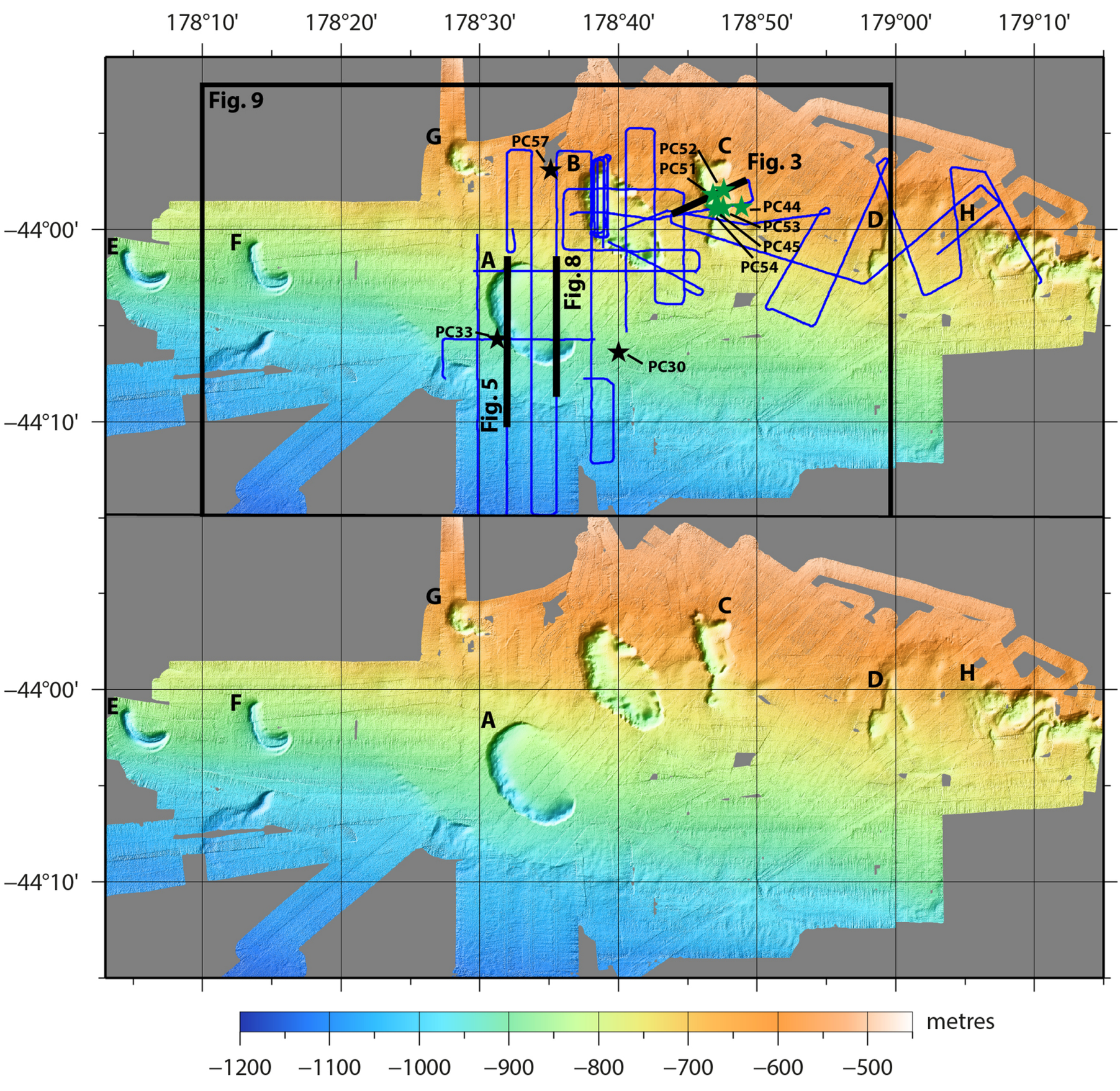
178°10'
178°20'
178°30'
178°40'
178°50'
179°00'
179°10'
−44°00'
−44°10'
Fig. 9
G
PC57
B
PC52
PC51
C
Fig. 3
PC44
PC53
PC45
PC54
D
H
E
F
A
Fig. 8
PC33
PC30
Fig. 5
metres
−1200
−1100
−1000
−900
−800
−700
−600
−500

Figure 2

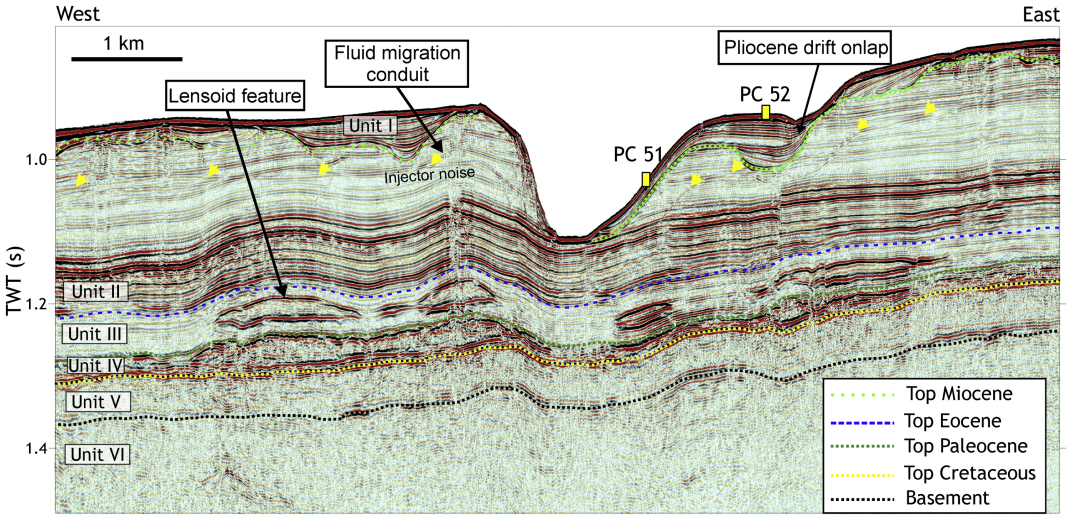
West
East
1 km
Fluid migration conduit
Lensoid feature
Pliocene drift onlap
PC 52
PC 51
Unit I
Injector noise
Unit II
Unit III
Unit IV
Unit V
Unit VI
TWT (s)
1.0
1.2
1.4
Top Miocene
Top Eocene
Top Paleocene
Top Cretaceous
Basement

Figure 3

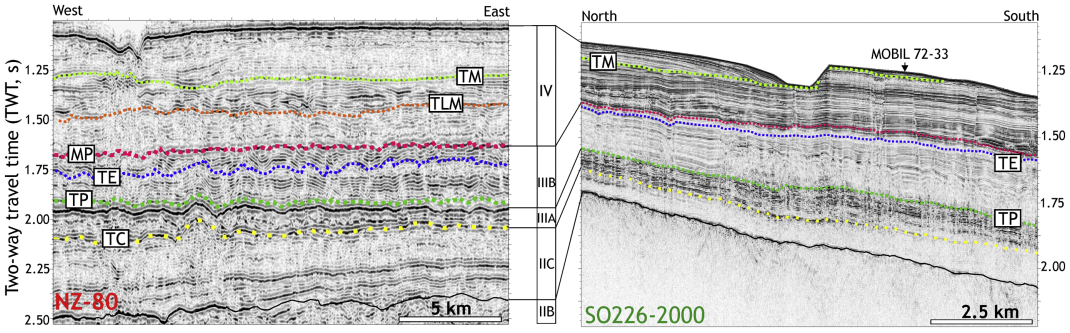
West
East
North
South
Two-way travel time (TWT, s)
1.25
1.50
1.75
2.00
2.25
2.50
TM
TLM
MP
TE
TP
TC
IV
IIIB
IIIA
IIC
IIB
NZ-80
5 km
MOBIL 72-33
SO226-2000
2.5 km

Figure 4

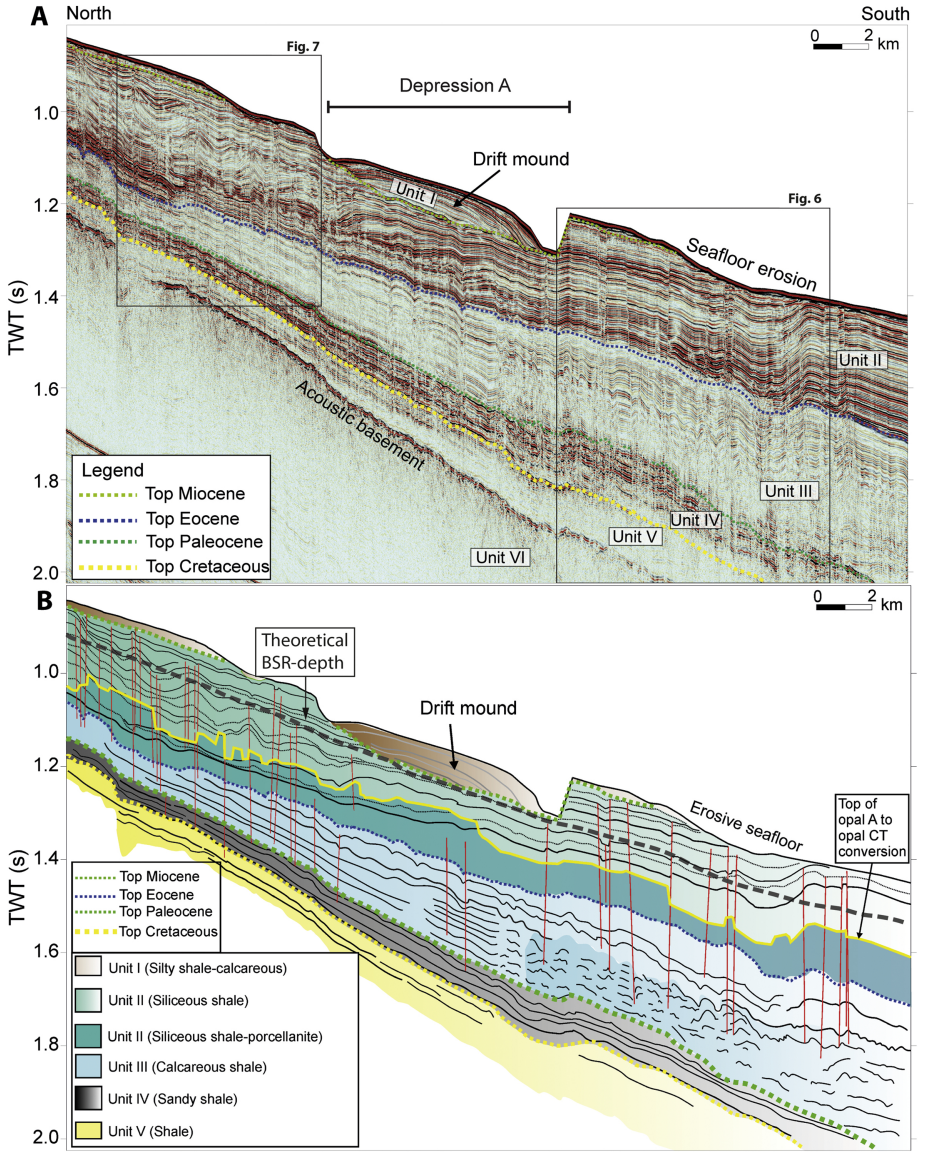
A
North
South
0 2 km
Fig. 7
Depression A
Drift mound
Unit I
Fig. 6
Seafloor erosion
Unit II
Unit III
Unit IV
Unit V
Unit VI
Acoustic basement
TWT (s)
1.0
1.2
1.4
1.6
1.8
2.0
Legend
Top Miocene
Top Eocene
Top Paleocene
Top Cretaceous
B
0 2 km
Theoretical BSR-depth
Drift mound
Erosive seafloor
Top of opal A to opal CT conversion
TWT (s)
Top Miocene
Top Eocene
Top Paleocene
Top Cretaceous
Unit I (Silty shale-calcareous)
Unit II (Siliceous shale)
Unit II (Siliceous shale-porcellanite)
Unit III (Calcareous shale)
Unit IV (Sandy shale)
Unit V (Shale)

Figure 5

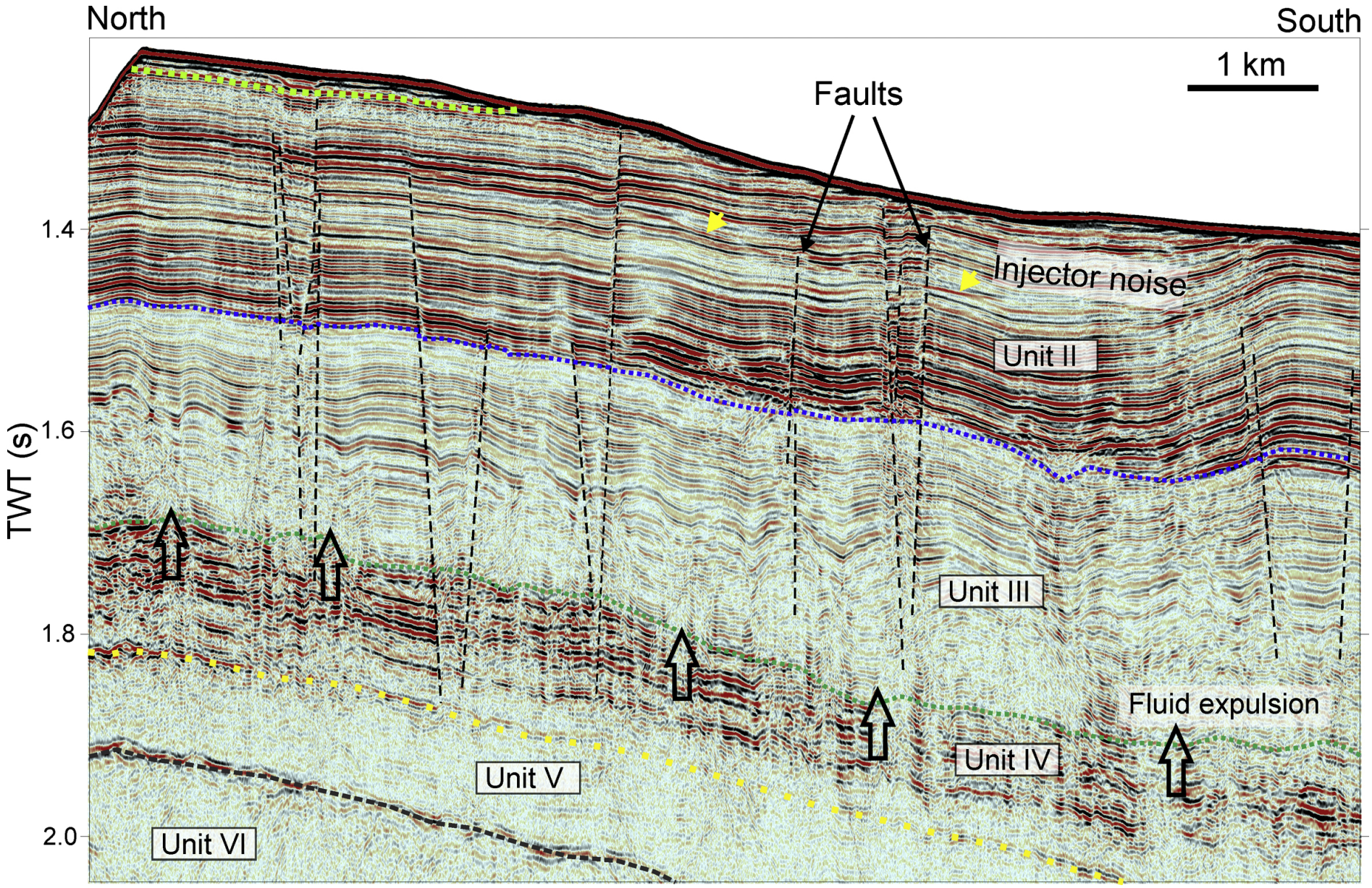
North
South
1 km
Faults
Injector noise
Unit II
Unit III
Unit IV
Unit V
Unit VI
Fluid expulsion
TWT (s)
1.4
1.6
1.8
2.0

Figure 6

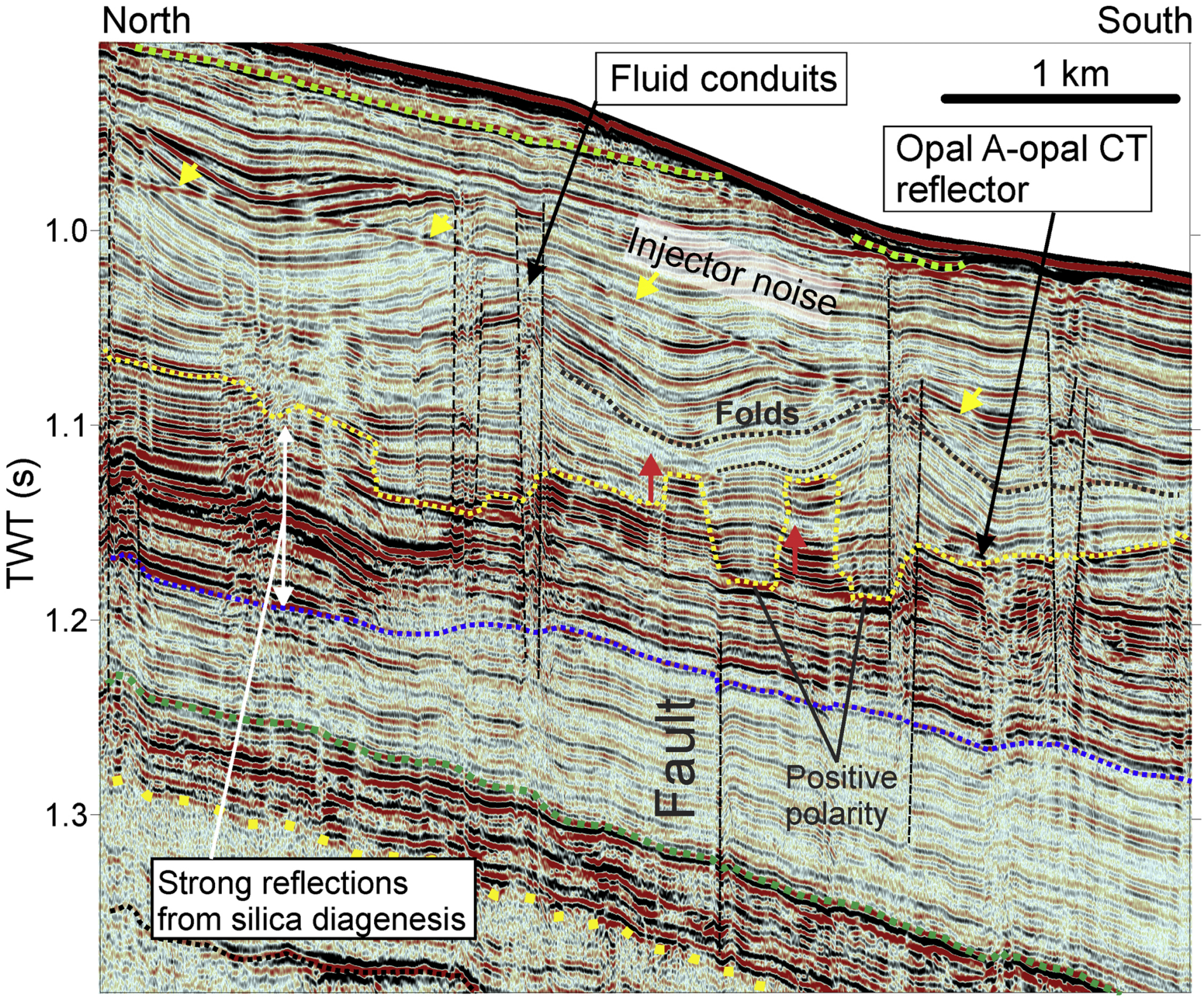
North
South
Fluid conduits
1 km
Opal A-opal CT reflector
Injector noise
Folds
Fault
Positive polarity
Strong reflections from silica diagenesis
TWT (s)
1.0
1.1
1.2
1.3

Figure 7

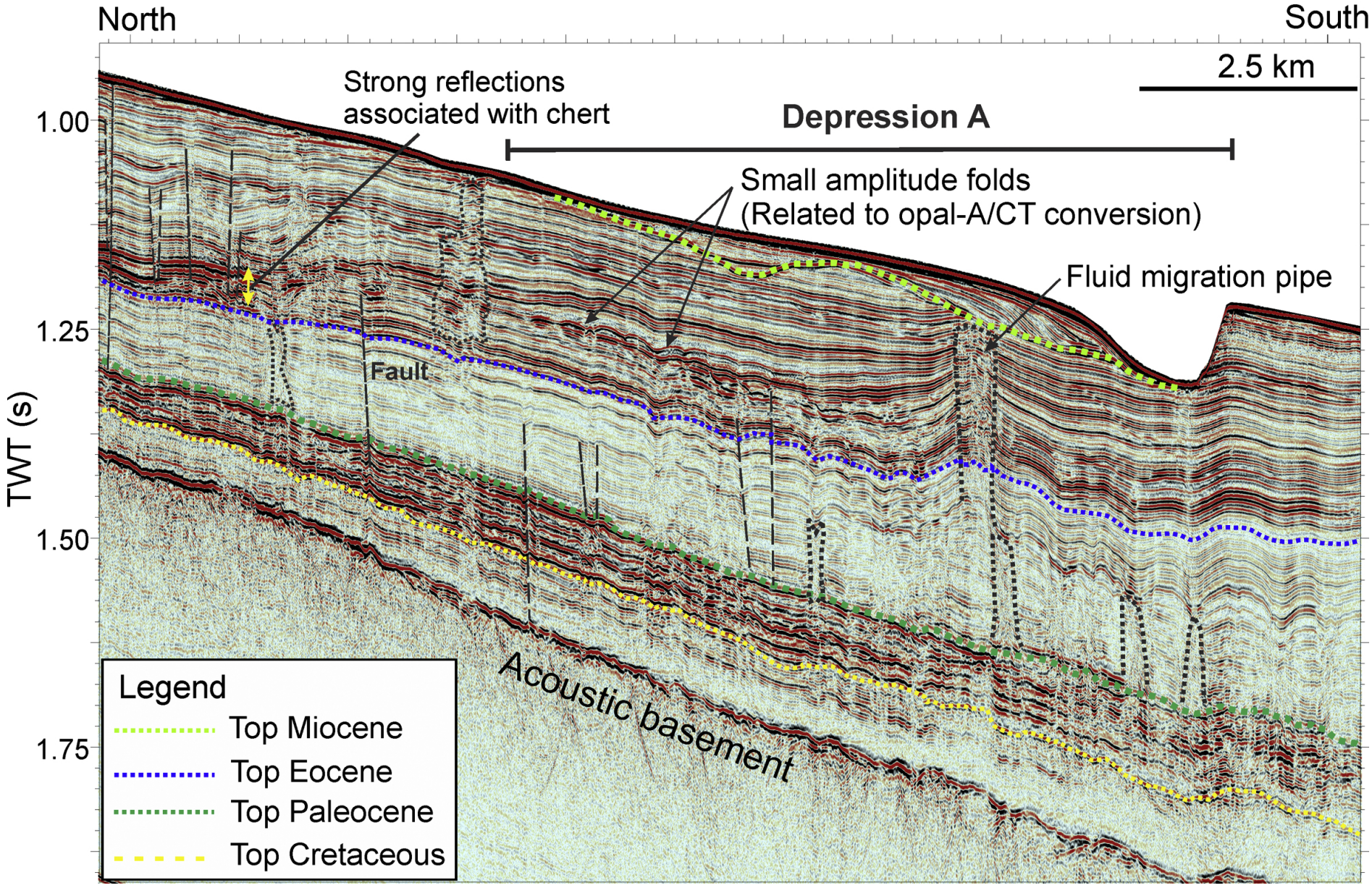
North
South
2.5 km
Strong reflections
associated with chert
Depression A
Small amplitude folds
(Related to opal-A/CT conversion)
Fluid migration pipe
Fault
Acoustic basement
TWT (s)
1.00
1.25
1.50
1.75
Legend
Top Miocene
Top Eocene
Top Paleocene
Top Cretaceous

Figure 8

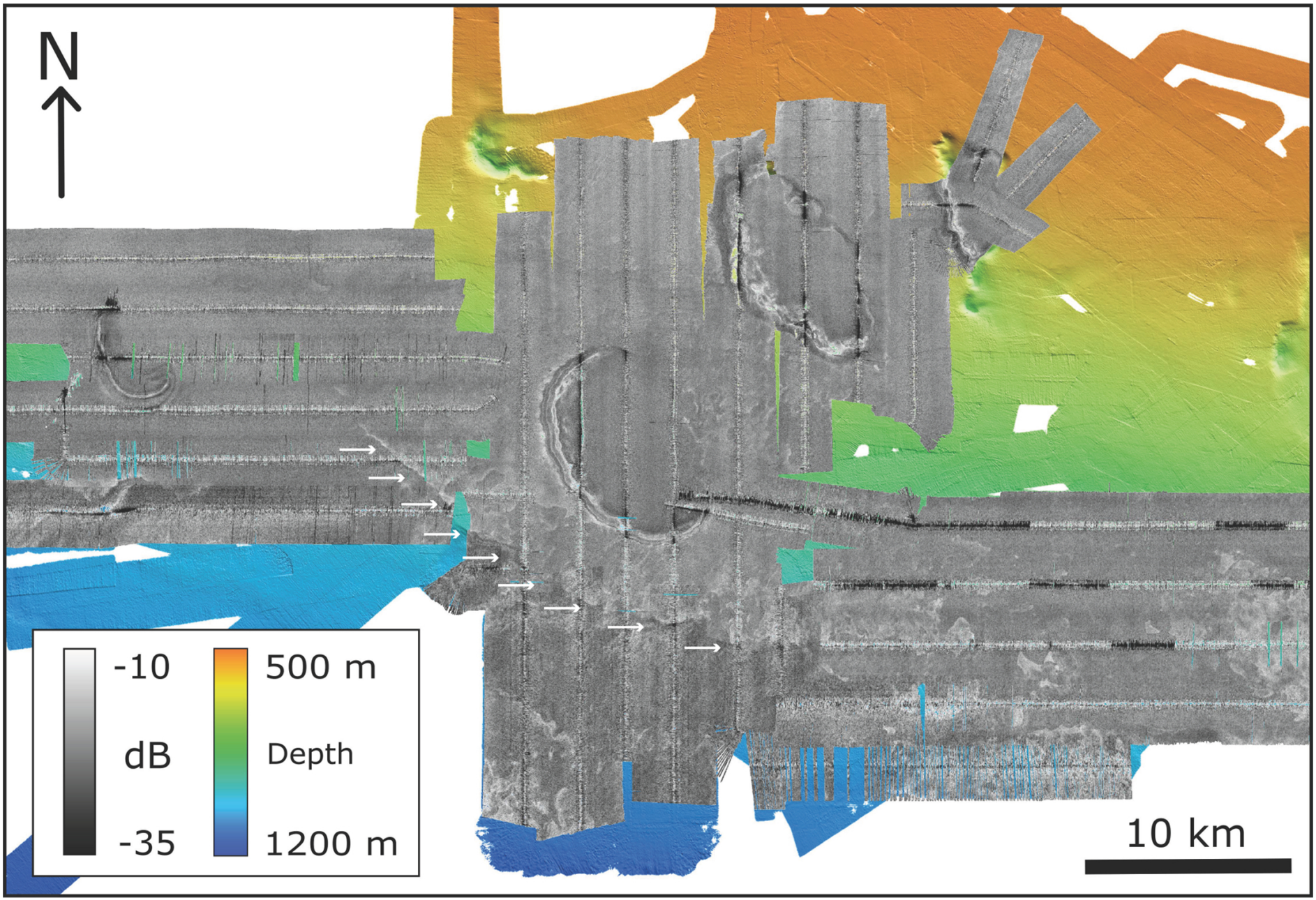

Figure 9

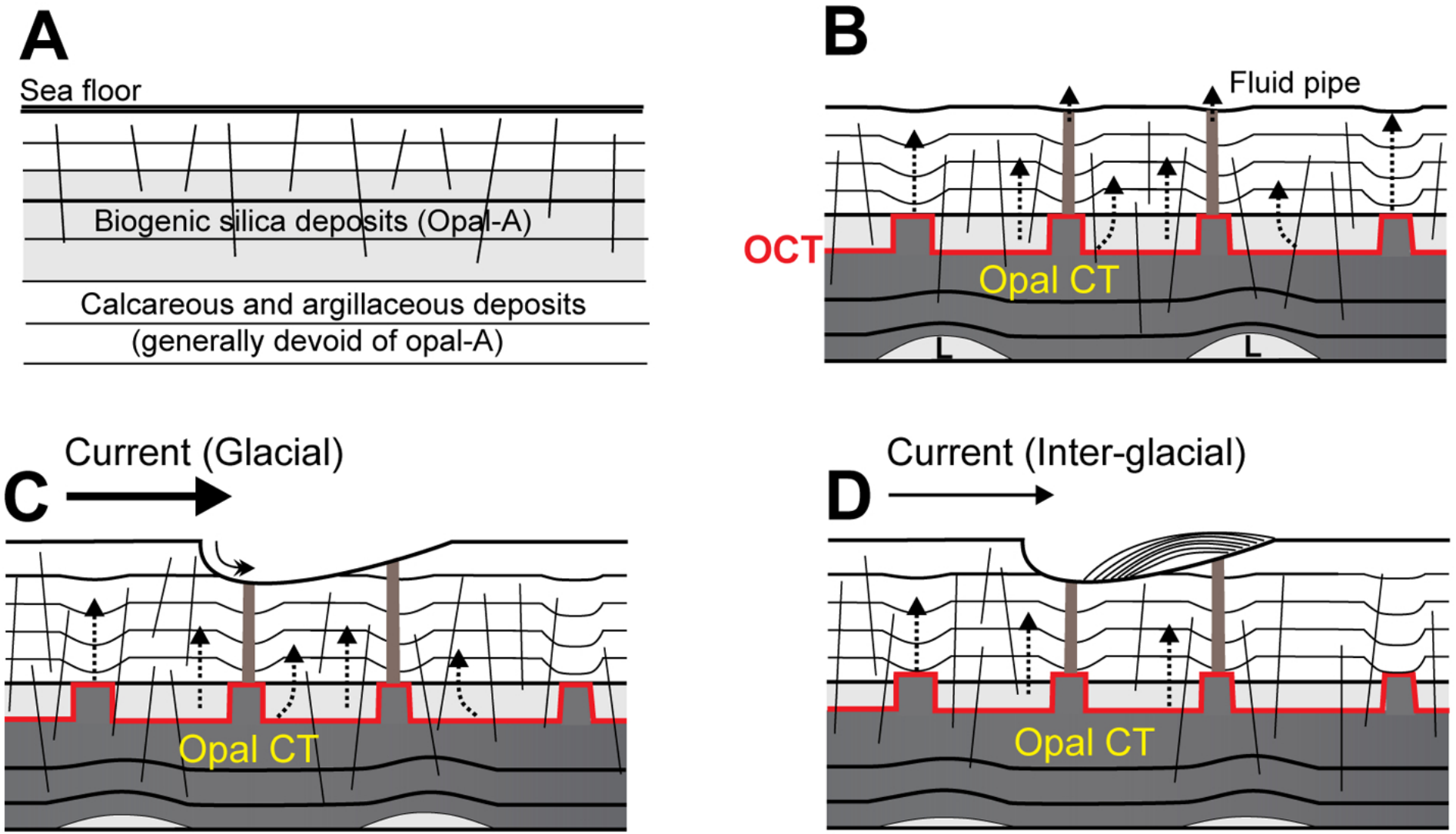
A
Sea floor
Biogenic silica deposits (Opal-A)
Calcareous and argillaceous deposits
(generally devoid of opal-A)
B
Fluid pipe
OCT
Opal CT
L
L
C
Current (Glacial)
Opal CT
D
Current (Inter-glacial)
Opal CT

Figure 10